Nature Communications

https://doi.org/10.1038/s41467-026-70300-x

Article in Press

Compact mid-infrared fiber probe for in vivo multi-compound monitoring demonstrated using ex vivo human skin

Received: 10 October 2025

Accepted: 23 February 2026

Cite this article as: Lee, T.-A., Hutter, T. Compact mid-infrared fiber probe for in vivo multi-compound monitoring demonstrated using ex vivo human skin. *Nat Commun* (2026). https://doi.org/10.1038/s41467-026-70300-x

Tse-Ang Lee & Tanya Hutter

Compact mid-infrared fiber probe for in vivo multi-compound monitoring demonstrated using ex vivo human skin

Tse-Ang Lee,[1] Tanya Hutter[1,2,*]

[1]Walker Department of Mechanical Engineering, The University of Texas at Austin, Austin, TX 78712, USA;
[2]Materials Science and Engineering Program and Texas Materials Institute, The University of Texas at Austin, Austin, TX 78712, USA

*Corresponding author: tanya.hutter@utexas.edu

ABSTRACT

Simultaneous monitoring of multiple biomarkers in tissues is critical for biomedical applications. However, few existing platforms enable concurrent *in vivo* detection. This study presents a compact mid-infrared transflection optical fiber probe for label-free, simultaneous monitoring of three physiologically relevant biomarkers – ethanol, glucose, and lactate. The probe comprises two silver halide fibers - one with an angled tip and one gold-coated as mirror - housed in polyetheretherketone tubing and surrounded by a semi-permeable membrane. With an outer diameter of only 1.1 mm, this is the smallest mid-infrared transflection probe reported to date. Coupled with quantum cascade laser, the probe achieves ~1 mM detection limits for the three compounds. Peak deconvolution was deployed to resolve overlapping spectral features, enabling quantification of individual compounds in mixtures. Validation was performed in *ex vivo* human skin against microdialysis. Additionally, monitoring of the concentration changes for all three compounds in the skin was demonstrated.

Keywords: Optical fiber probe, mid-infrared spectroscopy, silver halide fiber, ethanol, glucose, lactate, human skin

1. INTRODUCTION

Real-time monitoring or detection of small-molecule metabolites such as ethanol, glucose, and lactate is crucial for advancing precision medicine, early disease detection, managing metabolic disorders, guiding therapeutic decisions, and improving patient outcomes in critical care settings [1–4]. These molecules serve as important biomarkers across diverse physiological and pathological conditions; Glucose and lactate levels are used to assess brain metabolic dysfunction following traumatic brain injury (TBI), where elevated lactate and reduced glucose are associated with poor outcomes [5]. Continuous glucose monitoring is fundamental in diabetes management [6], while elevated lactate serves as a critical prognostic marker in sepsis [7]. Ethanol monitoring is important in contexts such as alcohol intoxication and addiction treatment [8]. Monitoring changes in concentration over time can help with better understanding of the metabolic pathway, which is important for developing new treatments and therapeutics. Ethanol metabolism also influences glucose and lactate dynamics due to hepatic metabolic competition and mitochondrial effects [9,10]. In scenarios such as ethanol-indued liver injury [11], simultaneous monitoring of ethanol, glucose, and lactate provides a more complete picture of the metabolic status. Table 1 summarizes clinical relevance

and applications of glucose, lactate and ethanol that underscore the importance of developing a sensing platform capable of measuring them simultaneously.

Conventional approaches, such as microdialysis, are widely used for *in vivo* and *ex vivo* monitoring of biochemical markers [25,26]. Microdialysis allows localized sampling of interstitial fluid for subsequent offline analysis [27,28], and thus inherently does not provide real-time continuous measurement and suffers from low temporal resolution due to slow perfusion rates and long sampling intervals. Additionally, accurate quantification of concentration in tissues requires tedious calibration procedures. Furthermore, this extraction-based technique can deplete molecules locally in the tissue surrounding the microdialysis probe, resulting in changes of the chemical environment and leading to lower concentrations in the collected sample. Electrochemical sensing, particularly through enzyme-based detection, is the primary approach for monitoring metabolites such as glucose and lactate, providing rapid, real-time measurements and integration into wearable and implantable devices [29–34]. Although effective, electrochemical sensors are limited by fouling and the need for immobilized enzymes with finite lifespans and degradation of the electrode [35]. Raman-based probes enable label-free detection with low interference from water; however, they typically require high excitation power and are susceptible to background fluorescence in biological media [36]. Although recent studies, such as an implantable near-infrared spectroscopy sensor [37], have demonstrated simultaneous monitoring of ethanol, glucose and lactate in biological tissue, these systems involve surgical implantation which increases the overall cost and the complexity of the procedure. Moreover, the relatively large device size, requiring an incision of approximately 3.5 cm for implantation, restricts its use to specific tissue sites and limits broader medical applicability.

Mid-infrared (IR) spectroscopy enables molecular detection in tissues by directly probing the fundamental vibrational fingerprints of molecular bonds. This approach allows chemical identification without the need for additional targeting markers and provides distinct spectral features that are not captured in the overtone-dominated near-IR region. Each compound shows unique absorbance peaks in the mid-IR region (wavelengths 2.5–20 μm, corresponding to wavenumbers 4000–500 cm^{-1}), which result from characteristic bond vibrations. This enables direct molecular identification and quantification. Several mid-IR sensing modalities have been explored for chemical sensing purpose; Attenuated total reflectance (ATR) spectroscopy, which measures evanescent-wave absorption from a sample in contact with a high-refractive index crystal, has been used for analyzing glucose [38,39], and lactate [40]. Due to the limited light-matter interaction, the sensitivity is generally lower than that of other approaches. Evanescent-wave fiber sensors utilize uncladded, bent or tapered mid-IR fibers - typically made from silver halide or chalcogenide materials - where the evanescent field extends beyond the fiber surface to interact with surrounding medium. Bending or tapering increases the extent of the evanescent field interacting with the sample, which enhances sensitivity. In a previous study [41], glucose was measured using a triple-coiled silver halide fiber sensor with a bend radius of 2.5 mm. Other studies have demonstrated the use of evanescent-wave sensors for detecting volatile organic compounds in aqueous environments [42], as well as for keratin quantification [43] and for distinguishing between healthy and cancerous skin tissue [44]. Fiber-optic sensors operating in transmission mode, where light passes directly through the sample between two aligned fibers, have been used to measure various concentration of glucose in different synthetic mixtures [45]. However, the implementation of evanescent-wave and transmission fiber sensors in tissues remains challenging, as their size and configuration can cause tissue damage (e.g., transmission measurements require alignment of two

fibers within the tissue). To minimize the invasive impact, alternative design for fiber probes, such as a transflection configuration, is preferable [46].

In this study, a transflection fiber probe operating in the mid-IR region with an average pathlength of 63 µm was developed. The mid-IR transflection fiber probe, which uses a quantum cascade laser (QCL) as its light source, has an overall diameter of 1.1 mm. The sensing area of the probe is surrounded with a semi-permeable membrane having pores of 2-5 nm to prevent direct contact of the silver halide fiber with the tissue to enhance biocompatibility. Additionally, the membrane excludes large particles such as cells and proteins from the sensing region, thus preventing biofouling and reducing potential interference in the IR measurement. The probe was first tested by measuring ethanol, glucose and lactate in aqueous solutions. The temporal response of the fiber probe was investigated in a glucose solution, comparing probes with and without a membrane. The performance of the probe was validated in a tissue by measuring ethanol concentration over time in *ex vivo* human skin against a standard technique for sampling small molecules in tissues – microdialysis. Additionally, ethanol, glucose and lactate concentrations were measured in the skin sample simultaneously to demonstrate the multi-compound sensing capability. Peak deconvolution of the measured spectra was performed to resolve overlapping spectral features to quantify the concentrations of each compound. A rapid injection–dilution experiment was performed to show that the probe is capable of capturing concentration changes in tissue with a temporal resolution of 30 seconds. To estimate chemical stability and biocompatibility of the fiber probe, the dissolution of silver halide fiber was measured in ultrapure water over 7 days. The results showed that the maximum silver ion concentration remained below 26 ppb. This design demonstrates a versatile platform for multi-compound sensing in a biologically relevant environment.

2. RESULTS AND DISCUSSION

2.1 FTIR spectroscopy of ethanol, glucose, and lactate in aCSF

To establish a reference for evaluating the performance of the fiber probe, mid-infrared absorbance spectra of ethanol, glucose, and lactate in artificial cerebrospinal fluid (aCSF) were measured using a benchtop Fourier-transform infrared (FTIR) spectrometer equipped with a 50 µm pathlength liquid transmission cell. aCSF was selected as the solvent to simulate the ionic environment of biological fluids.

Figures 1(a), 1(b), and 1(c) show the absorbance spectra of ethanol, glucose, and lactate, respectively, measured over the spectral range of 1000–1180 cm^{-1}. All compounds were measured at concentrations between 2.5 and 40 mM. The spectrum of aCSF was used as the background for absorbance calculation. Ethanol has two prominent C–O stretching bands at 1046 and 1088 cm^{-1}, consistent with previous literature [49]. Glucose shows multiple peaks, resulting from C–O stretching vibrations, as expected, the peak positions are centered at 1036, 1066, 1082, 1110, and 1154 cm^{-1} [50]. Lactate presents three distinguishable peaks centered around 1042, 1086, and 1124 cm^{-1}. The peak at 1042 cm^{-1} corresponds to C-C stretching, and the peaks at 1086 and 1124 are corresponding to C–O stretching vibrations [51].

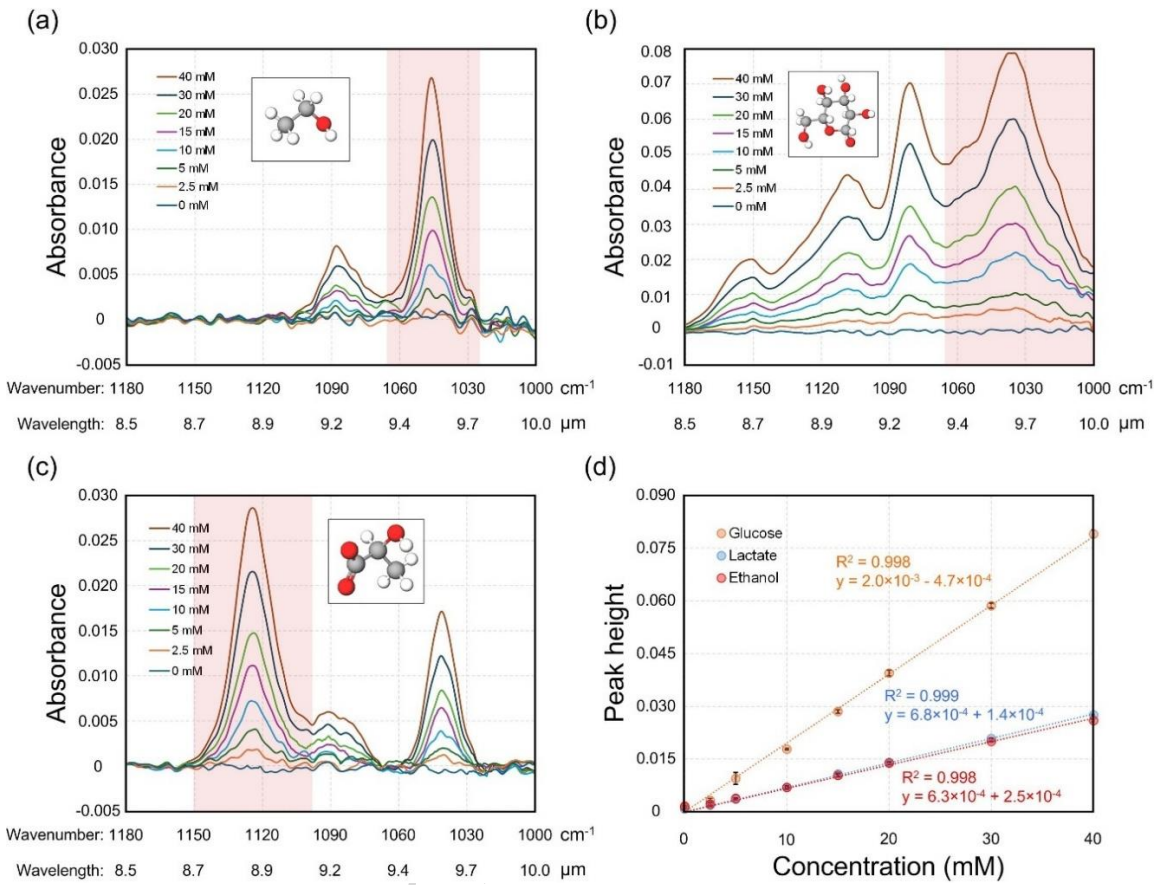

Figure 1. FTIR spectroscopy and calibration of ethanol, glucose and lactate. FTIR absorbance spectra of (a) ethanol, (b) glucose and (c) lactate in aCSF at various concentrations between 2.5 and 40 mM measured with a pathlength of 50 µm. (d) Calibration curve showing peak heights versus concentration for each compound. Error bars represent the standard deviation (N=3).

For quantification, a single absorbance peak was selected for each compound based on the signal intensity and linear response to concentration. Specifically, 1046 cm^{-1} was used for ethanol, 1036 cm^{-1} for glucose, and 1124 cm^{-1} for lactate as indicated by the red shaded regions. The peak heights were determined by fitting Gaussian functions to the experimental spectra using nonlinear least-squares curve fitting, as described in Section 2.10. The calibration curves shown in Figure 1(d) demonstrate strong linearity across the tested concentration range, with correlation coefficients (R^2) exceeding 0.99 for all three compounds. The sensitivities, defined as the slope of the calibration curves, for ethanol, glucose and lactate are 6.3×10^{-4} 1/mM ± 5.7%, 2.0×10^{-3} 1/mM ± 3.7%, 6.8×10^{-4} 1/mM ± 4.9%, respectively. The uncertainties correspond to the relative standard error calculated from three measurements. Among the three, glucose has the highest slope in the calibration curve, reflecting its stronger mid-IR absorption due to its higher number of interacting chemical bonds. Lactate showed a slightly steeper slope than ethanol.

The limits of detection (LoD), calculated as three times the standard deviation of the blank divided by the calibration slope, were 1.8 mM ± 5.4% for ethanol, 1.3 mM ± 4.0% for glucose, and 1.2 mM ± 3.7% for lactate. These results confirm the capability of mid-IR spectroscopy to detect these biologically relevant

molecules in aqueous environments at physiologically meaningful concentrations, as summarized in Table 1.

2.2 Measurement of ethanol, glucose, and lactate solutions using the transflection fiber probe

To evaluate the performance of the developed mid-infrared transflection fiber probe for chemical sensing in aqueous biological environments, ethanol, glucose, and lactate dissolved in artificial cerebrospinal fluid (aCSF) were measured and directly compared with the FTIR results.

Figures 2(a), 2(b), and 2(c) present the absorbance spectra of ethanol, glucose, and lactate, measured using the fiber probe with an average optical pathlength of 63 μm. The same characteristic peaks identified in the FTIR reference measurements were used for quantification: 1046 cm^{-1} for ethanol (C–O stretch), 1036 cm^{-1} for glucose (C–O stretch), and 1124 cm^{-1} for lactate (C–O stretch), as indicated by the red shaded regions. The peak heights were extracted by Gaussian fitting, as in the FTIR measurements. Figure 2(d) shows the corresponding calibration curves for all three compounds, each showing linearity with R^2 values exceeding 0.99. The sensitivities for ethanol, glucose and lactate are 4.3×10^{-4} 1/mM ± 3.3%, 9.4×10^{-4} 1/mM ± 2.8% and 4.5×10^{-4} 1/mM ± 4.0%, respectively. The uncertainties correspond to the relative standard error calculated from three measurements. Notably, glucose again has the highest sensitivity among the three compounds. Lactate showed a slightly higher sensitivity than ethanol, with a difference of approximately 5%. Although the fiber probe has a longer geometric pathlength than the FTIR flow cell, it has lower sensitivities for ethanol, glucose and lactate measurements. The reported 63 μm optical path length corresponds to the geometric spacing between the angled fiber tip and the gold-coated fiber. However, the effective optical path length may be shorter. In addition, refractive-index differences among the analyte solutions can slightly alter refraction and reflection at the interfaces, resulting in analyte-dependent variations in sensitivity. These effects are fully accounted for through the calibration curves.

The limits of detection (LoD), determined as three times the standard deviation of the blank divided by the calibration slope, were 1.0 mM ± 3.1% for ethanol, 0.81 mM ± 2.7% for glucose, and 1.1 mM ± 3.7% for lactate. These values are lower than those obtained from the benchtop FTIR setup (see Section 3.1). Despite lower sensitivity, the fiber probe achieved better limits of detection than the FTIR system, which may be attributed to the high intensity QCL light source, which enables better signal-to-noise ratios. To identify the main source of noise in the fiber-probe system, 10 repeated background spectra with the probe in air and 10 spectra with the laser output measured directly at the detector were recorded. The standard deviation at each wavenumber was calculated and normalized by the corresponding mean intensity to obtain the relative noise. The average relative noise over the 1000–1180 cm^{-1} region was 0.025% for the direct laser measurement and 0.078% for the fiber-probe. The result indicates that, compared to detector and laser noise, propagation and coupling in the silver halide fiber contribute the majority of the overall noise in the system.

One key advantage of the transflection probe is its suitability for *in vivo* environment. Unlike FTIR transmission cells, which require samples to be contained within a flow cell, the fiber probe interacts directly with the surrounding medium, making it ideal for *in situ* measurements in tissue.

These results confirm that the mid-IR transflection fiber probe offers sensitive detection of small biomolecules in aqueous environment, and provides a promising platform for biochemical sensing, especially in settings where traditional FTIR setups are impractical.

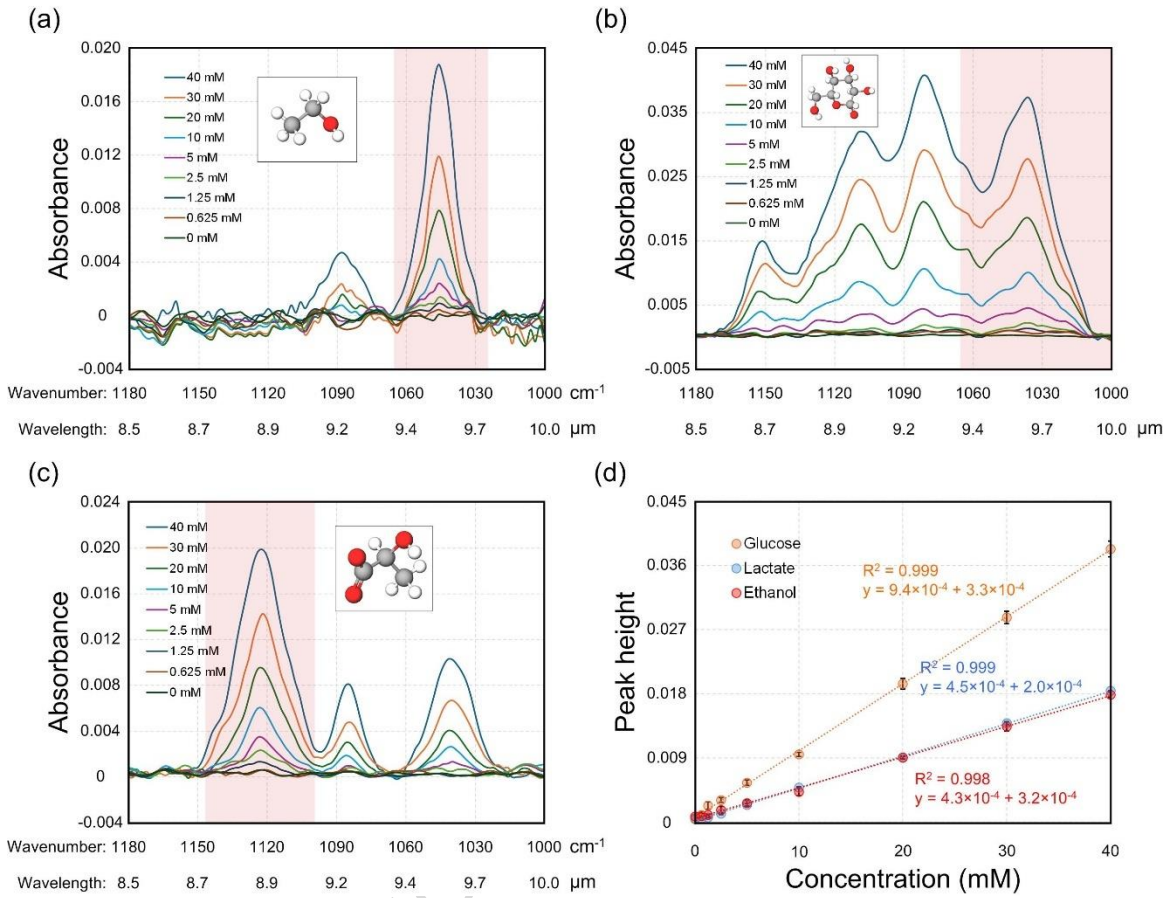

Figure 2. Transflection fiber probe measurements and calibration of ethanol, glucose and lactate. Absorbance of (a) ethanol, (b) glucose, and (c) lactate in aCSF measured using the mid-IR transflection fiber probe with an averaged optical pathlength of 63 μm. (d) Calibration curve showing peak height versus concentration for each compound. Error bars represent the standard deviation (N=3)

2.3 Simultaneous quantification of mixture of ethanol, glucose, and lactate using peak deconvolution

To demonstrate the capability of simultaneously measuring multiple compounds, mixtures of ethanol, glucose, and lactate in aCSF were measured and analyzed. The same fiber probe with an average optical pathlength of 63 μm was used. Three spectral scans were averaged for each measurement, resulting in a total acquisition time of 1.5 minutes. Peak deconvolution was applied to resolve overlapping absorbance features and quantify each component.

Figure 3(a) shows the mid-IR absorbance spectrum of a mixture containing 20 mM of ethanol, 20 mM of glucose, and 20 mM of lactate and the Gaussian fits for each compound where the position of peaks were identified based on prior FTIR calibration (Section 3.1). In the spectra of mixture, Gaussian functions were fitted at 1046 and 1088 cm^{-1} for ethanol; at 1036, 1066, 1082, 1110, and 1154 cm^{-1} for glucose; and at 1042, 1086, and 1124 cm^{-1} for lactate. To quantify each compound in the mixture, the specific peak heights of the Gaussian functions at 1046, 1036, and 1124 cm^{-1} were extracted for ethanol, glucose and lactate, respectively. The concentrations were determined using the calibration curves in Figure 2(d). The combined

fit achieved an R^2 of 0.995, indicating good agreement between the measured spectrum and the sum of individual spectral contributions.

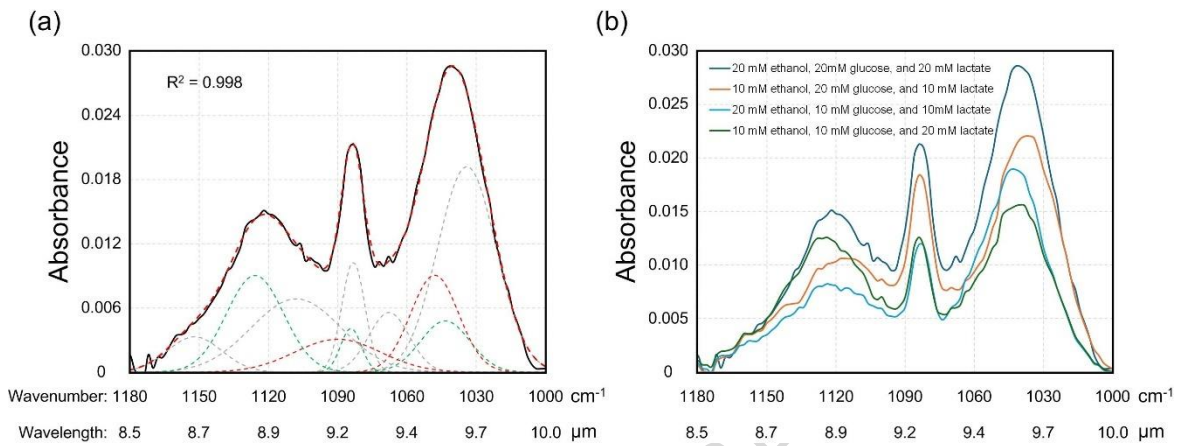

Figure 3. Quantification of mixture of ethanol, glucose and lactate using peak deconvolution. (a) Absorbance spectrum of a mixture containing 20 mM ethanol, 20 mM glucose, and 20 mM lactate measured using the fiber probe with an averaged optical pathlength of 63 μm, overlaid with the peak deconvolution fit. (b) Absorbance spectra of three different mixtures with varying concentrations of glucose, lactate and ethanol used to validate the deconvolution method.

To validate the peak deconvolution method, three standard mixtures containing different known concentrations of each compound were tested as summarized in Table 2. Figure 3(b) shows the corresponding infrared spectral features of these standard mixtures. The average relative prediction errors, defined as the percentage difference between the predicted and actual concentrations relative to actual concentration, for ethanol, glucose and lactate in the three standard mixtures were 10.8%, 5.2% and 3.3%, respectively, demonstrating that quantitative multicomponent analysis is feasible with the developed fiber probe. Additionally, the accuracy of ethanol quantification was slightly more variable, which may be due to peak overlap with both lactate and glucose. Lactate showed the highest accuracy, likely due to its characteristic peak being separated from those of other compounds, resulting in less spectral interference. Glucose quantification was also reliable, with deviations typically below 1 mM across all conditions.

However, due to spectral overlap, the use of peak deconvolution introduces greater uncertainty into the concentration measurements compared to single-component analysis. In single-compound measurements, the signal originates from a single compound, and the quantification relies on direct peak fitting. In contrast, when multiple compounds are present, their spectra overlap in the mid-IR region, leading to shared spectral features and baseline shifts. Deconvolution algorithm resolves these overlapping peaks by fitting multiple parameters, such as peak height and width, for each compound simultaneously. This process increases the degrees of freedom in the fitting model, which in turn propagates fitting errors and increases the variability of predicted concentrations.

Table 3 shows the relative standard error (RSE) of the peak heights used for quantifying ethanol, glucose, and lactate. The peak heights used to calculate the RSEs were measured both individually and within

mixtures at concentrations of 10 and 20 mM. For all three compounds, the RSE is consistently higher in the multi-compound measurements compared to single-component analysis. For instance, ethanol shows an RSE increase from 3.4% to 8.9% at 10 mM and from 2.3% to 5.9% at 20 mM when comparing single to multi-compound detection. This trend is observed for glucose and lactate as well. The magnitude increase is smaller for lactate, likely due to its more isolated spectral peaks. This increase in RSE directly affects the LoD for each compound in mixtures. The LoD is defined as three times the standard deviation of the measurement divided by the slope of the calibration curve. As the standard deviation increases due to uncertainties in deconvolution, the LoD for multi-compound measurements becomes higher than that for single-compound measurements, even if the calibration slope remains similar. As a result, while the fiber probe demonstrates feasibility for simultaneous multi-compound sensing, the achievable detection limits in mixtures are higher than those in single-component analyses (1.0, 0.8, and 1.1 mM for glucose, ethanol and lactate) due to the uncertainty introduced by peak overlap and deconvolution fitting.

These findings highlight the potential of the fiber probe for simultaneous multi-compound quantification, without the need for prior sample processing or the use of markers to target the molecules. This capability is particularly valuable in biological contexts where monitoring of metabolic markers such as glucose and lactate, along with ethanol, may offer insights into tissue health and metabolic state. However, this capability comes with the trade-off of higher detection limits when resolving complex mixtures through peak deconvolution. Advanced chemometric and machine-learning approaches such as partial least squares (PLS) or principal component regression could be implemented in future studies to improve sensitivity and reduce analytical variance in multi-compound measurements.

2.4 Probe's performance with and without a semi-permeable membrane

In addition to considerations related to sensor dimensions and ability to quantify concentrations using IR, biofouling - the attachment of cell debris or adsorption of proteins on the fiber - can deteriorate the performance of the sensor. Additionally, previous literature have noted potential biocompatibility concerns for bare silver halide fibers in direct contact with cells [52]. This effect can be mitigated through including a semi-permeable membrane or surface coating [52]. Additionally, a semi-permeable membrane or coating can prevent direct contact of the silver halide fiber to the tissue to prevent potential risk of biocompatibility. A mPES membrane was chosen for this purpose. Its hydrophilic nature helps prevent bubble formation, and its 10 kDa MWCO allows diffusion of small molecules but blocks large particles such as proteins. However, with the membrane, the diffusion dynamics of ethanol, glucose and lactate may change. Two experiments were conducted to investigate the effect of membrane on the sensitivity (slope of the calibration curve) and the response time of the fiber probe, respectively.

In the first experiment, glucose calibration curve was measured following the procedure in Section 3.2 using the same probe with and without a semi-permeable membrane around the sensing region. Measurements were started at least 5 minutes after each sample change to ensure that steady-state concentrations were reached. Figure 4(a) shows the calibration curves for glucose in aCSF, measured both with and without the membrane. The sensitivities of the probe with and without a membrane were 9.4×10^{-4} 1/mM ± 2.0% and 9.4×10^{-4} 1/mM ± 2.2%, respectively. The uncertainties correspond to the relative standard error calculated from three measurements. Difference between the two curves is within 1%. Similar sensitivity with and without membrane is expected, as 5 minutes is sufficient to reach steady-state concentration, as verified in the following section discussing the temporal response of the probe. This also

applies to ethanol and lactate, since these smaller molecules diffuse faster than glucose. Consequently, the results demonstrate that the probe performs effectively, despite the presence of the membrane.

In the second experiment, temporal response studies were conducted to examine the effect of a semi-permeable membrane on the fiber probe. Absorbance of 20 mM glucose was monitored over time with a single-scan acquisition time of 25 seconds, both in the presence and absence of the membrane. These experiments evaluate the sensor's capacity to monitor dynamic concentration changes.

In both conditions, fiber probe with an average optical pathlength of 63 μm was used. The fiber was initially immersed in a vial of aCSF to record baseline signals ($t < 0$). At $t = 0$, the vial was changed to another vial containing 20 mM glucose. After a defined period, the vial was changed back to aCSF to observe the signal decay over time. The response curves are shown in Figure 4(b) and Figure 4(c) for the probe without a membrane and the membrane-protected probe, respectively. The response was quantified by calculating the time constant, defined as the time required for the signal to reach 90% of its maximum (rise).

For the probe without a membrane, the response was faster, with a time constant of 33.4 seconds ± 5.4%. In contrast, the membrane-protected probe showed a slower response, with a time constant of 59.1 seconds ± 5.9%. The increase in response time reflects the added diffusion resistance introduced by the membrane. The semi-permeable membrane will help with filtering out large macromolecules and particles, potentially reducing biofouling and signal interference, but it slows the transport of molecules to the sensing region. Despite the slower response, the membrane-protected probe still reached 90% of the steady-state signal within one minute, indicating that real-time monitoring remains feasible for many applications.

The decay curves after switching back to aCSF also support these findings. The decay time constants, defined as the times required for the signal to decrease to 10% of the maximum (when immersed in glucose solution), were 36.1 seconds ± 5.5% and 61.7 seconds ± 4.7% for probe with and without a membrane, respectively. The unprotected probe showed a sharp drop in signal, returning near baseline within 1 minute. In comparison, the membrane-equipped probe displayed a more gradual signal decay, consistent with residual glucose diffusing out of the membrane-protected sensing zone.

Overall, these results demonstrate that while the membrane reduces the rate of mass transfer, and thus slightly compromising the temporal response, the concentration changes of ethanol, glucose and lactate changes in the human body is typically occur slowly enough to be captured with a temporal resolution of 1 minute [53–55]. The choice of using a membrane should depend on the specific application requirements, whether fast response or selective filtering is prioritized.

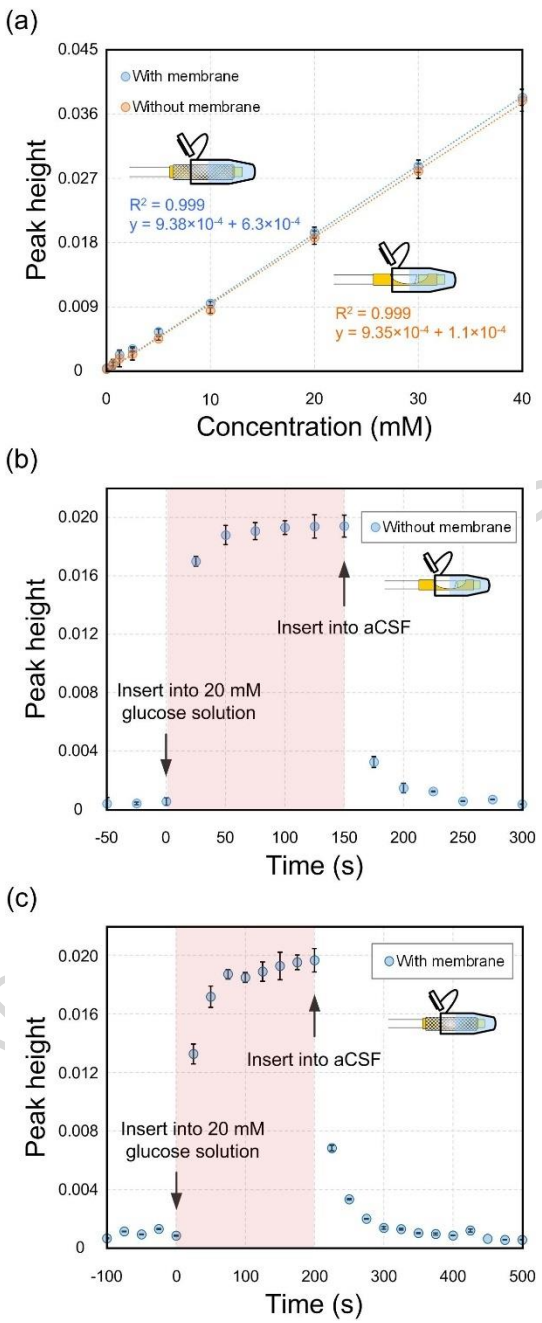

Figure 4. Performance comparison with and without a semi-permeable membrane. (a) Calibration curves for glucose in aCSF obtained using the probe with and without the semi-permeable membrane. Time-course infrared peak height at 1036 cm^{-1} of 20 mM glucose measured using the fiber probe (b) without and (c) with a semi-permeable membrane. The shaded region indicates the period when the probe was immersed in the glucose solution. Error bars represent the standard deviation (N=3).

2.5 *Ex vivo* skin measurement using the fiber probe and comparison with microdialysis

To compare the performance of the fiber probe and microdialysis, concentrations in *ex vivo* human skin were monitored by both techniques following ethanol spiking of the medium under the skin. The mid-IR fiber probe (with a semi-permeable membrane and an averaged optical pathlength of 63 μm) and the microdialysis probe were inserted into the same skin sample, positioned at depths of 2.7 and 2.9 mm, respectively. Ethanol was added to the culture medium at t=0 to achieve a final concentration of 20 mM. Figure 5(a) shows the ethanol concentrations measures by both techniques over time. The concentrations increased after ethanol addition, with the rate of increasing slowing approximately 30 minutes later. The temporal concentration profiles reflect the gradual penetration of ethanol into the skin. The fiber probe measured a maximum tissue concentration of approximately 8 mM, which is lower than the spiked medium concentration, as expected. This discrepancy is due to diffusion barriers within the skin and underlying nourishing matrix, which slows down the transport process of ethanol to the region where the probes were embedded. Compared to microdialysis, which operates at a low perfusion rate (0.5 μL/min) and requires a 10-minute sampling interval, the fiber probe provides better temporal resolution, allowing faster tracking of concentration changes over time. Additionally, the concentration measured using microdialysis was slightly lower than those obtained with the fiber probe. This may be attributed to the evaporation losses of ethanol during sample collection and handling required for the microdialysis process. Moreover, because the molecules diffused into the microdialysis probe were continuously carried to the sample collection vial at outlet, local depletion of molecules in the surrounding tissue can occur. This is a limitation not encountered with the non-extractive, in situ sensing mechanism of the fiber probe.

To demonstrate the fiber probe's capability for measuring mixtures in ex vivo human skin, the culture medium beneath the skin sample was spiked with 100 mM ethanol, 100 mM glucose and 100 mM lactate and their concentrations were measured over time. As shown in Figure 5(b), all three compounds were simultaneously detected using peak deconvolution. Each compound has a distinct temporal concentration profile, even though their initial spiked concentrations were the same. Ethanol showed the highest concentration, while glucose and lactate showed lower levels. These differences result from their distinct diffusion coefficients of each molecule within skin tissue. Ethanol, due to its small size, diffuses more easily through both the nourishing matrix and the skin tissue above it compared to glucose and lactate. As a result, the steady-state concentration of ethanol is higher than that of glucose and lactate. Among the three, glucose is the largest molecule, leading to the slowest diffusion rate and the lowest steady-state concentration. Additionally, the skin cells in the samples remain metabolically active and use glucose for energy. However, the metabolic demand of the skin tissue is relatively small compared to the large glucose reservoir provided in the medium. As a result, any glucose consumption during the 90-minute measurement period would be too small to detect, which is consistent with the experimental results shown in Figure 5(b).

To evaluate the temporal response of the fiber probe in capturing dynamic concentration changes, ethanol spectra were collected every 30 seconds using single-scan acquisition to minimize measurement time. Figure 5(c) shows measurements of ethanol concentration over time following the injection of 50 μL of 200 mM ethanol into the skin near the probe at t = 0 min. A quick increase in measured concentration was observed within the first 10 minutes. At t = 30 min, 20 μL of culture medium was added directly on the skin near the probe to quickly dilute the local ethanol concentration. The corresponding decrease was detected by the fiber probe. The results underscore the capability of the fiber probe to capture concentration variations on sub-minute timescales.

Overall, these findings highlight two main advantages of the mid-IR fiber probe over microdialysis: (1) in situ measurement without the need for sample extraction or processing, (2) high temporal resolution suitable for capturing dynamic changes. These features make the developed probe a promising tool for *in vivo* molecular monitoring in tissues. Future work will focus on further miniaturing both the probe and the overall measurement system, enhancing the probe's sensitivity and validating its performance in *in vivo* models to advance toward clinical applications. A key challenge is replacing the current large infrared laser system and optical components with portable alternatives. Identifying suitable light sources and detectors that balance size, sufficient power, and cost-effectiveness will be critical for translating this technology into practical, handheld devices.

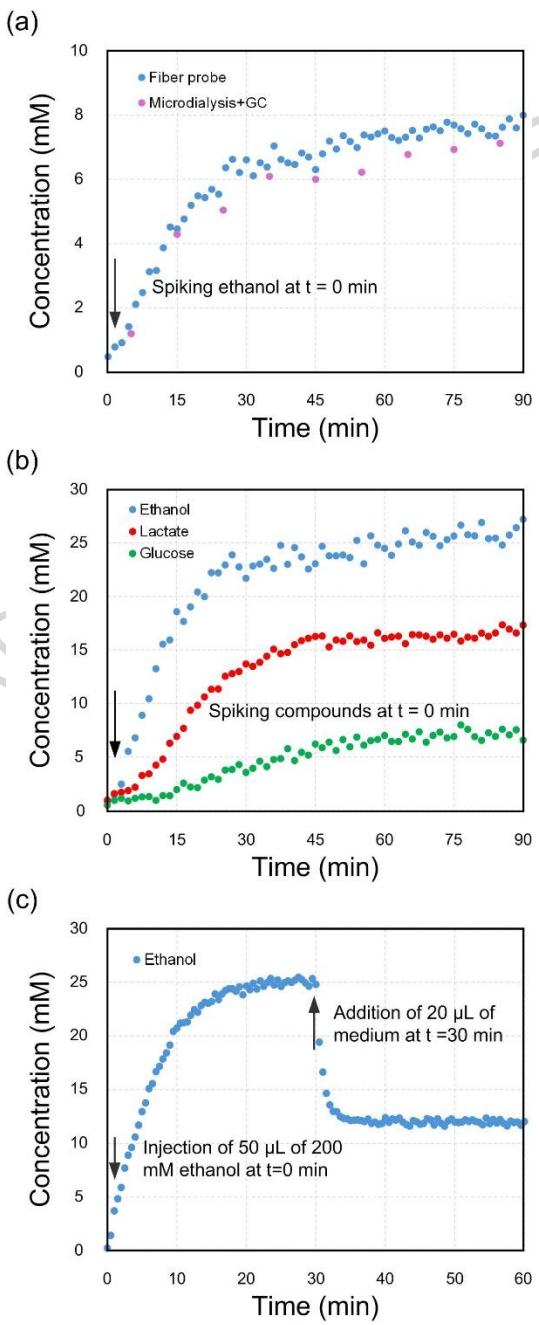

Figure 5. Fiber probe measurements in *ex vivo* skin and comparison with microdialysis. (a) Time-course comparison of ethanol measurements in the skin samples using fiber probe and microdialysis. Ethanol was spiked into the medium at t = 0 min to achieve a final concentration of 20 mM. (b) Simultaneous monitoring of ethanol, glucose, and lactate in the skin sample, with the medium spiked at 100 mM for each compound. (c) Monitoring of ethanol dynamics in the skin sample following the injection of 50 μL of 200 mM ethanol at t = 0 min. A rapid increase in ethanol concentration was observed, followed by dilution at t = 30 min with the addition of 20 μL of medium.

2.6 Evaluation of silver ion release and biocompatibility considerations

To assess the potential risk of the release of ions from the silver halide fiber in the probe for biological applications, the dissolution of silver halide in aqueous environments was investigated. The concentration of silver ions was measured as an indicator of the extent of fiber dissolution. This was quantified by immersing a fiber probe with a semi-permeable membrane in ultrapure water for 7 days. Samples were collected daily and analyzed using an ICP-MS.

As shown in Figure 6, the measured silver ion concentration remained low throughout the test period, with a maximum concentration below 26 ppb. The control sample, prepared before fiber immersion, showed an undetectable silver ion concentration (0 ppb), confirming minimal background contamination. The highest concentration of silver ions is well below known cytotoxic thresholds and is considered safe for biomedical applications. Toxicity effects are generally reported at levels around 1000 ppb for human fibroblasts [56]. In addition, the amount of dissolved chloride and bromide ions can be estimated based on the measured silver ion concentration, as these halide ions are released in stoichiometric proportions during the dissolution of the silver halide material. Therefore, the concentrations of chloride and bromide ions are expected to be lower than the silver ion levels detected in the solution. Notably, the physiological concentrations of chloride and bromide ions in human body are substantially higher than these levels [57,58], further indicating that the small quantities potentially released from the fiber probe are unlikely to pose a health risk.

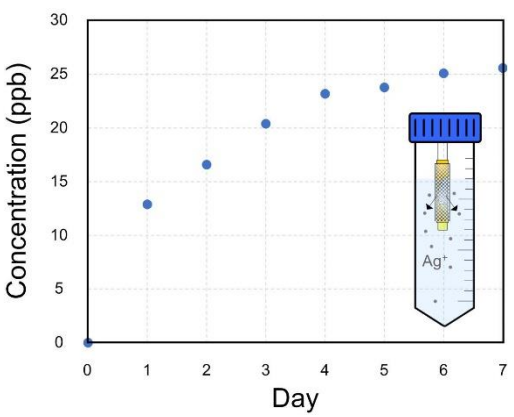

Figure 6. Silver ion concentration released from the silver halide fiber probe with a semi-permeable membrane immersed in ultrapure water over seven days.

In the proposed probe design, a semi-permeable PES membrane encloses the entire sensing region, creating a physical barrier that further prevents direct tissue contact with the silver halide fiber, which can enhance the overall biocompatibility of the device. Based on the low silver ion concentrations measured and the use of the membrane, the results support the potential use of the probe in short-term *ex vivo* and *in vivo* applications Future work will focus on long-term evaluations of the effect of silver halide fiber probe on tissue, to ensure safe use *in vivo*.

3. METHODS

3.1 Optical fiber

Uncladded polycrystalline silver halide fibers (PIR 500, Art Photonics, Germany), composed of a solid solution of silver chloride and silver bromide, were used to fabricate the fiber probes. The fiber has a diameter of 500 µm, a numerical aperture (N.A.) of 0.3, and is transparent in the wavelength range of 3 to 17 µm, with transmission rate above 55% in the 8–10 µm range for a 1 m length and an optical loss of 0.2-0.3 dB/m in the 9-13 µm range.

3.2 Reagents

An artificial cerebrospinal fluid (aCSF) was prepared to simulate the chemical and ionic composition of the interstitial fluid, according to a previous study [47]. The concentration of each component was as follows: NaCl at 149 mM (S9888, Sigma), KCl at 2.8 mM (409316, Fluka), $CaCl_2 \cdot 2H_2O$ at 1.2 mM (21097, Sigma), $MgSO_4 \cdot 6H_2O$ at 1.2 mM (63068, Sigma), ascorbic acid at 0.25 mM (95209, Fluka), glucose at 5.4 mM (G7021, Sigma). 200 proof ethanol (111000200, PHARMCO), glucose (G7021, Sigma) and lactate (L7022, Sigma) were used to prepare standard solutions in aCSF through serial dilution.

3.3 Skin tissue models

Abdominal skin (NativeSkin, Genoskin) collected from a 31-year-old Hispanic female donor after plastic surgery was split into multiple samples used for testing probe performance *ex vivo*. The skin samples have a diameter of 20 mm and a thickness of approximately 4.6 mm. Each skin biopsy is contained in a cell culture insert designed to fit standard six-well plates. The insert has a porous membrane at its base, allowing nutrient exchange between the culture medium and the skin tissue. A nourishing gel-like matrix of proprietary composition is positioned between the membrane and the skin, providing physical support and keeping the tissue chemically stable. A silicone ring circles the exposed surface of the skin, preventing the applied liquids from leaking into the culture medium. As a result, the working area of the skin surface is reduced to 1.76 cm^2. The skin sample was received one day after production. Upon delivery, the skin samples were refreshed with new medium and kept in culture at least 3 hours prior to experiment. Experiments were performed in accordance with the manufacturer's instructions and before the expiration date of the tissue. This study is not classified as human subject research, and no Institutional Review Board approval was required. Product certification from the manufacturer can be provided upon request.

3.4 Fourier-transform infrared spectroscopy (FTIR)

A Fourier-transform infrared (FTIR) spectrometer (Nicolet is50, Thermo Scientific), equipped with a liquid cell (Oyster, Specac) operating in transmission mode, was used to measure solutions of ethanol, glucose and lactate as a reference method. The liquid cell has an optical pathlength of 50 µm and CaF_2 windows, requiring a sample volume of 10 µL. The number of scans was 300, resulting in spectra collection time of

187 seconds, and the spectral resolution was 0.482 cm^{-1}. The spectrum of aCSF was used as the background for absorbance calculations in the experiments.

3.5 Headspace gas chromatography with flame ionization detector (GC-FID)

A gas chromatograph (GC, 430-GC, Bruker) equipped with a flame ionization detector (FID) and an autosampler (COMBI PAL-xt) was used to analyze the concentration of ethanol in the dialysate samples. CompassCDS (Bruker, Netherlands) software was used to record and analyze all chromatograms. A capillary column (30 m x 0.53 mm x 1 μm film thickness) with nitrogen as the mobile phase, at a flow rate of 8.5 mL/min, was used. A carboxen/PDMS coated solid phase micro-extraction (SPME) fiber (Supelco Analytical, Bellefonte, PA) was used for extraction and desorption. The extraction time was set to 3 minutes, followed by a desorption period of 1 minute. The oven and injection temperature were maintained at 65 ^{o}C and 220 ^{o}C, respectively.

3.6 Fabrication of microdialysis probes

Microdialysis probes were assembled in a side-by-side configuration, following the procedure described in a prior study [47]. Briefly, two pieces of fused silica tubing used as the inlet and outlet lines and were inserted into a segment of regenerated cellulose membrane (132280, Spectra/Por) with a 13 kDa molecular weight cutoff (MWCO), which corresponds to an effective pore size of 2-5 nm [48]. The active dialysis region was determined by adjusting the relative insertion lengths of the tubing inside the membrane and was set to 2 mm. Epoxy was applied externally to coat the region that is not used for dialysis.

3.7 Fabrication of optical fiber probes

Figure 7(a) illustrates the schematic design of the mid-infrared transflection fiber probe. The probe consists of two aligned silver halide optical fibers. One fiber is used for light delivery and collection, and the other serves as a reflective mirror. The fiber mirror was fabricated by coating the end-face of a short segment of silver halide fiber with a gold layer of approximately 267 nm thickness, using a sputter coater (6002, Ted Pella, Inc.). Before gold sputtering, the fiber end was polished using aluminum oxide lapping film (50-20060, Allied High Tech Products, Inc.). The other fiber, used for delivery and collection of the IR light, was polished at a 7° angle on its end face facing the fiber mirror using a custom-made fiber holder. This angled fiber tip helps reduce Fresnel back reflections by redirecting the reflected light away from the fiber core.

Both fibers were held and aligned face-to-face inside a custom-fabricated connector made from a 6 mm-long hollow polyetheretherketone (PEEK) tube (1532L, IDEX Health and Science) with an inner diameter of 510 μm and an outer diameter of 1588 μm. The outer surface of the PEEK tube was machined down to an outer diameter of approximately 850 μm to fit within a semi-permeable membrane (modified polyethersulfone (mPES), 10 kDa MWCO corresponding to effective pore size of around 3 nm). The alignment of the two fibers was adjusted under a microscope to control the optical pathlength – twice the distance between the two fibers. The average optical pathlength of the fiber probe was 63 μm, which is twice the average distance between the fiber tip and the fiber mirror. This average distance was determined by measuring the shortest and longest distances between the angled fiber tip and the fiber mirror under a microscope and calculating their mean. The space between the fiber tip and the fiber mirror defines the sensing region, which requires a sample volume of 13 nL to fill completely. To enable molecules to reach the sensing region, a 2 mm-wide groove was created in the PEEK tube along the wall using a hand drill. The fiber probe was inserted into a 3 mm-long piece of the semi-permeable membrane enclosing the tube

and covering the sensing window and secured using epoxy at both ends. This configuration allows small molecules to diffuse through the membrane into the sensing region while excluding large particles such as proteins. The overall outer diameter of the final probe is 1.1 mm. The photograph of the final assembled probe is shown in Figure 7(b). Before measurement, the probe was pre-wetted with a 25% ethanol solution, which wets the narrow sensing gap due to its lower surface tension and displaces any trapped air. The probe was then immersed in water for at least 15 minutes to allow the ethanol to diffuse out prior to use. This procedure ensures that the sensing region is fully filled with liquid and free of air bubbles during experiments.

3.8 Optical setup

Figure 7(c) shows the schematics of the experimental setup. A mid-infrared quantum cascade laser (QCL, MIRcat, DRS Daylight Solutions) was used as the light source, delivering a spectral range of 800–1800 cm^{-1} (5.56–12.5 μm). A focusing coupler (Art Photonics GmbH), consisting of a gold mirror (39-193, Edmund Optics) and an off-axis parabolic mirror (35-488, Edmund Optics), was installed at the laser output, as shown in the schematics. The mirror mounted inside the focusing coupler features three adjustment screws for fine-tuning the x, y, and z positions, enabling signal optimization at the FC-PC connector output.

The output of the focusing coupler was connected to one input of a fiber splitter (Art Photonics GmbH), which combined two silver halide fibers (500 μm diameter) for delivering the laser light and transmitting the return signal to the detector, as illustrated in the schematics. The two fibers of the splitter were bundled together into a single fiber cable, which was connected to the transflection probe through an SMA connector. The fiber lengths were 23 cm for both the source-to-SMA connector and detector-to-SMA connector paths, and 5 cm from the SMA connector to the sensing region. The fiber splitter provides an approximately 50/50 division of the optical signal between the two fibers. To connect the transflection probe to the fiber splitter, a 3D-printed hollow cylinder was fabricated with an inner diameter matching that of the fiber probe for secure insertion, and an outer diameter designed to tightly fit the SMA connector port. The signal carrying spectral information was directed to a thermoelectrically cooled infrared detector (PVI-4TE-10.6, VIGO Photonics) using a dual-mirror fiber coupler (Art Photonics GmbH). This coupler consists of two off-axis parabolic mirrors (MPD229-P01, ThorLabs) that collect and focus the light onto the detector, as illustrated in the schematic.

3.9 *Ex vivo* skin measurements

To assess the performance of the mid-IR transflection fiber probe, *ex vivo* experiments were conducted using human abdominal skin samples. For direct comparison of the fiber probe and microdialysis, both the optical fiber probe and a lab-made microdialysis probe were inserted into the dermis of the same skin sample, positioned approximately 2.7 mm and 2.9 mm below the top skin surface, respectively, as shown in Figure 7(d). Insertion of both probes was performed by first making a small incision in the dermis using a scalpel, followed by piercing the tissue with a 27-gauge needle to create a tract for the probes. The fiber and microdialysis probes were then carefully inserted along this path.

The fiber probe was used to acquire mid-IR spectra *in situ*, while the microdialysis probe served as a reference method for sampling extracellular molecules. The culture insert, which contains skin tissue, placed in a six-well plate containing medium, was kept inside a humidified incubator at 37°C for the duration of the experiments. The microdialysis system included a syringe pump delivering artificial cerebrospinal fluid (aCSF) at a constant perfusion rate of 0.5 μL/min. Dialysate was collected in vials at

10-minute intervals. A 2 μL aliquot from each dialysate sample was transferred to a glass vial for subsequent analysis using GC-FID.

To directly compare the measurement results of the fiber probe and the microdialysis probe, both were inserted in the skin sample, and ethanol concentration measurements were initiated simultaneously upon spiking the culture medium with ethanol to a concentration of 20 mM. During this experiment, spectra were acquired every 1.5 minutes, corresponding to an average of 3 scans, which provided sufficient noise reduction while maintaining the ability to resolve concentration changes on the timescale of diffusion through the skin tissue. The total experiment duration was 90 minutes, allowing both the initial rapid increase in analyte concentration and the subsequent approach to steady state within the tissue to be captured. The results obtained with both techniques are presented and compared in the first paragraph of Section 3.5.

For simultaneous multi-compound quantification, only the optical fiber was inserted in the skin sample. The medium was spiked with a mixture of 100 mM ethanol, 100 mM glucose, and 100 mM lactate. These high concentrations in the medium were used in order to achieve physiologically relevant concentrations in the dermis of the skin. Spectra were acquired every 1.5 minutes, and the acquired spectra were analyzed using peak deconvolution to resolve and quantify the overlapping absorbance features. The results of simultaneous multi-compound quantification are presented in the second paragraph of Section 3.5.

To evaluate the fiber probe's capability for capturing dynamic changes in concentration, an injection experiment was performed with the fiber probe in the tissue, as shown in Figure 7(e). A volume of 50 μL of 200 mM ethanol was injected into the skin at a site approximately 3 mm from the probe, followed by a dilution step in which 20 μL of culture medium was added directly at the insertion site of the probe to quickly reduce the local ethanol concentration. During this experiment, spectra were acquired every 30 seconds using single-scan acquisition to minimize measurement time. The results of tracking ethanol concentration over time are presented in the third paragraph of Section 3.5.

3.10 Spectral processing and peak deconvolution

All infrared absorbance spectra were processed and analyzed using MATLAB (R2023a, The MathWorks, Inc.). The spectra were first smoothed using a moving average method with a window size of 9 points. This window size was chosen to preserve peak shape and intensity while reducing high-frequency noise. Following smoothing, baseline correction was performed. An asymmetric least squares algorithm was used to estimate and subtract the baseline. This method iteratively minimizes a cost function that balances how closely the baseline follows the data and the smoothness of the estimated baseline. The two parameters, penalization and asymmetry parameters, were tuned empirically to achieve effective baseline correction across the spectral range of 1000–1180 cm^{-1}.

To resolve overlapping spectral features and quantify individual compounds, peak deconvolution was performed using nonlinear least-squares curve fitting with Gaussian functions. Each compound (ethanol, glucose, and lactate) was characterized by a predefined set of characteristic peaks, identified from measured infrared absorbance spectra of individual compounds using the fiber probe and validated with the reference FTIR spectra. The positions of the peaks were fixed based on experimental calibration using fiber probe, while the amplitude and width were allowed to vary during fitting. The peak height of each fitted Gaussian function was used for concentration quantification. Calibration curves relating peak height to concentration were generated for each compound.

To predict the concentration of each compound in the mixture, peak deconvolution was performed using all the characteristic peaks from the absorbance spectra of the pure compounds. The concentrations were then estimated using the corresponding calibration curve. Goodness-of-fit was assessed by calculating the coefficient of determination (R^2) between the experimental and fitted spectra.

3.11 Investigation of silver halide fiber dissolution

To evaluate the potential biocompatibility risks associated with the silver halide fiber probe, a dissolution study to measure the release of silver ions over time was conducted. A fully assembled fiber probe was submerged in 12 mL of ultrapure water and stored at room temperature for 7 days. 1 mL of the solution was withdrawn every day. Prior to analysis, each collected sample was diluted to a final volume of 5 mL with ultrapure water and acidified with nitric acid (HNO_3) to a final concentration of 2% (v/v), as required for inductively coupled plasma–mass spectrometry (ICP-MS) measurements.

The concentration of silver ions in the samples was quantified using an ICP-MS (Agilent Technologies) in solution mode. A baseline control sample (ultrapure water before the insertion of probe) was included to confirm background levels.

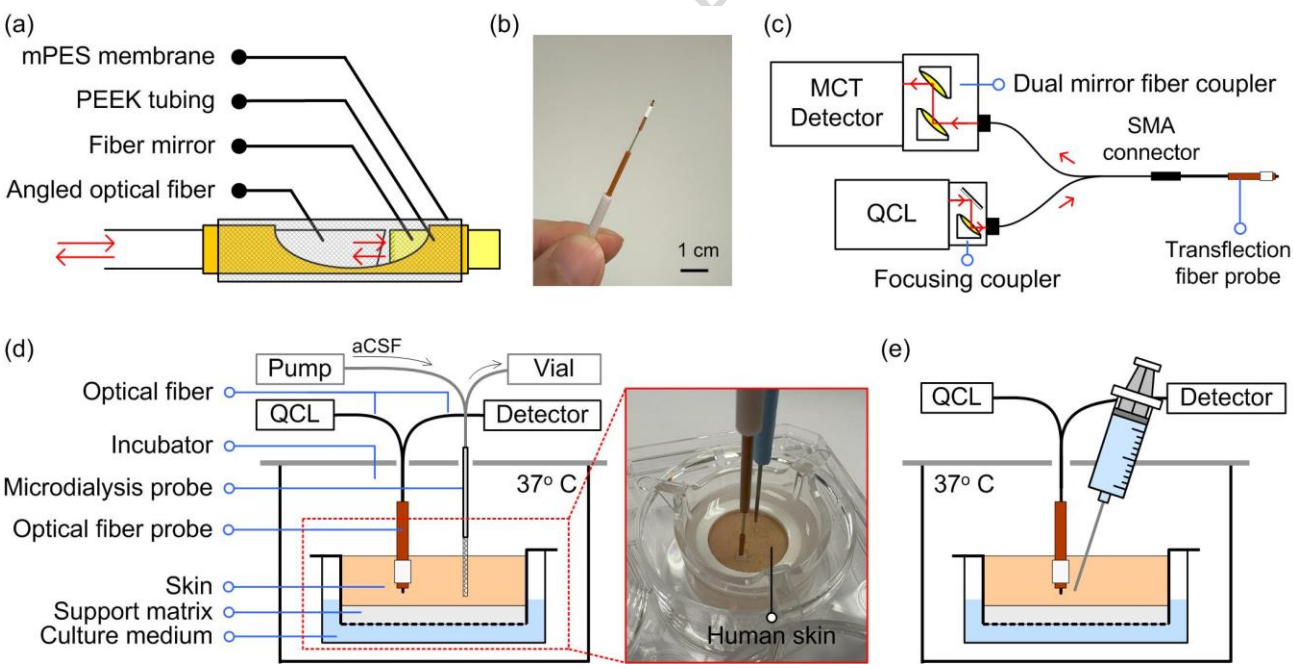

Figure 7. Schematic of the transflection fiber probe and experimental setup. (a) Configuration of the transflection fiber probe. (b) Photograph of the probe. (c) Schematic of the optical setup for the transflection probe measurements. (d) Schematic of the experimental setup using *ex vivo* skin. Both the transflection fiber probe and lab-made microdialysis probe were inserted into the dermis and secured in place, with the setup maintained at 37°C. The photograph on the right shows the fiber probe (left) and microdialysis probe (right) inserted in the human skin sample inside the cell culture insert. (e) Schematic of the injection experiment, where ethanol was injected into the skin near the probe.

DATA AVAILABILITY

Data underlying the results presented in this paper are not publicly available at this time but may be obtained from the authors upon request.

REFERENCES

[1] C.B. Clish, Metabolomics: an emerging but powerful tool for precision medicine, Cold Spring Harb. Mol. Case Stud. **1** a000588 (2015).

[2] G.N. Gowda, Zhang ,Shucha, Gu ,Haiwei, Asiago ,Vincent, Shanaiah ,Narasimhamurthy, D. and Raftery, Metabolomics-based methods for early disease diagnostics, Expert Rev. Mol. Diagn. **8** 617–633 (2008).

[3] Juvenile Diabetes Research Foundation Continuous Glucose Monitoring Study Group, W.V. Tamborlane, R.W. Beck, B.W. Bode, B. Buckingham, H.P. Chase, R. Clemons, R. Fiallo-Scharer, L.A. Fox, L.K. Gilliam, I.B. Hirsch, E.S. Huang, C. Kollman, A.J. Kowalski, L. Laffel, J.M. Lawrence, J. Lee, N. Mauras, M. O'Grady, K.J. Ruedy, M. Tansey, E. Tsalikian, S. Weinzimer, D.M. Wilson, H. Wolpert, T. Wysocki, D. Xing, Continuous glucose monitoring and intensive treatment of type 1 diabetes, N. Engl. J. Med. **359** 1464–1476 (2008).

[4] P. Deulkar, A. Singam, V.N.K.S. Mudiganti, A. Jain, Lactate Monitoring in Intensive Care: A Comprehensive Review of Its Utility and Interpretation, Cureus **16** e66356 (2024).

[5] A. Lozano, F. Franchi, R.J. Seastres, M. Oddo, O. Lheureux, R. Badenes, S. Scolletta, J.-L. Vincent, J. Creteur, F.S. Taccone, Glucose and Lactate Concentrations in Cerebrospinal Fluid After Traumatic Brain Injury, J. Neurosurg. Anesthesiol. **32** 162 (2020).

[6] G. Cappon, M. Vettoretti, G. Sparacino, A. Facchinetti, Continuous Glucose Monitoring Sensors for Diabetes Management: A Review of Technologies and Applications, Diabetes Metab. J. **43** 383–397 (2019).

[7] J. Chertoff, M. Chisum, B. Garcia, J. Lascano, Lactate kinetics in sepsis and septic shock: a review of the literature and rationale for further research, J. Intensive Care **3** 39 (2015).

[8] S. Paprocki, M. Qassem, P.A. Kyriacou, Review of Ethanol Intoxication Sensing Technologies and Techniques, Sensors **22** 6819 (2022).

[9] R.A. Kreisberg, A.M. Siegal, W.C. Owen, Glucose-lactate interrelationships: effect of ethanol, J. Clin. Invest. **50** 175–185 (1971).

[10] H.A. Krebs, R.A. Freedland, R. Hems, M. Stubbs, Inhibition of hepatic gluconeogenesis by ethanol, Biochem. J. **112** 117–124 (1969).

[11] J. Polson, W.M. Lee, American Association for the Study of Liver Disease, AASLD position paper: the management of acute liver failure, Hepatol. Baltim. Md **41** 1179–1197 (2005).

[12] K.P. Abrahao, A.G. Salinas, D.M. Lovinger, Alcohol and the Brain: Neuronal Molecular Targets, Synapses, and Circuits, Neuron **96** 1223–1238 (2017).

[13] Z.M. Weil, J.D. Corrigan, K. Karelina, Alcohol Use Disorder and Traumatic Brain Injury, Alcohol Res. Curr. Rev. **39** 171–180 (2018).

[14] G. Freund, Chronic Central Nervous System Toxicity of Alcohol, Annu. Rev. Pharmacol. Toxicol. **13** 217–227 (1973).

[15] K. Zierler, Whole body glucose metabolism, Am. J. Physiol.-Endocrinol. Metab. **276** E409–E426 (1999).

[16] T.A. Tirone, F.C. Brunicardi, Overview of Glucose Regulation, World J. Surg. **25** 461–7 (2001).

[17] I. Jalloh, K.L.H. Carpenter, A. Helmy, T.A. Carpenter, D.K. Menon, P.J. Hutchinson, Glucose metabolism following human traumatic brain injury: methods of assessment and pathophysiological findings, Metab. Brain Dis. 30 615–632 (2015).

[18] N.S. Chandel, Glycolysis, Cold Spring Harb. Perspect. Biol. **13** (2021) a040535. https://doi.org/10.1101/cshperspect.a040535.

[19] B. Phypers, J.T. Pierce, Lactate physiology in health and disease, Contin. Educ. Anaesth. Crit. Care Pain **6** (2006) 128–132. https://doi.org/10.1093/bjaceaccp/mkl018.

[20] R.S. de O. Cruz, R.A. de Aguiar, T. Turnes, R. Penteado Dos Santos, M. Fernandes Mendes de Oliveira, F. Caputo, Intracellular Shuttle: The Lactate Aerobic Metabolism, Sci. World J. **2012.1** 420984 (2012).

[21] L. Gattinoni, F. Vasques, L. Camporota, J. Meessen, F. Romitti, I. Pasticci, E. Duscio, F. Vassalli, L.G. Forni, D. Payen, M. Cressoni, A. Zanella, R. Latini, M. Quintel, J.J. Marini, Understanding Lactatemia in Human Sepsis. Potential Impact for Early Management, Am. J. Respir. Crit. Care Med. **200** 582–589 (2019).
[22] M. Masyuk, B. Wernly, M. Lichtenauer, M. Franz, B. Kabisch, J.M. Muessig, G. Zimmermann, A. Lauten, P.C. Schulze, U.C. Hoppe, M. Kelm, J. Bakker, C. Jung, Prognostic relevance of serum lactate kinetics in critically ill patients, Intensive Care Med. **45** 55–61 (2019).
[23] R.L. Veech, R. Guynn, D. Veloso, The time-course of the effects of ethanol on the redox and phosphorylation states of rat liver, Biochem. J. **127** 387–397 (1972).
[24] N.T. Broskey, K. Zou, G.L. Dohm, J.A. Houmard, Plasma Lactate as a Marker for Metabolic Health, Exerc. Sport Sci. Rev. **48** 119–124 (2020).
[25] C. Bjorkli, C. Louet, T.H. Flo, M. Hemler, A. Sandvig, I. Sandvig, In Vivo Microdialysis in Mice Captures Changes in Alzheimer's Disease Cerebrospinal Fluid Biomarkers Consistent with Developing Pathology, J. Alzheimer's Dis. **84** 1781–1794 (2021).
[26] F. Le Prieult, E. Barini, L. Laplanche, K. Schlegel, M. Mezler, Collecting antibodies and large molecule biomarkers in mouse interstitial brain fluid: a comparison of microdialysis and cerebral open flow microperfusion, mAbs **13** 1918819 (2021).
[27] B.-U. Moon, M.G. de Vries, C.A. Cordeiro, B.H.C. Westerink, E. Verpoorte, Microdialysis-Coupled Enzymatic Microreactor for in Vivo Glucose Monitoring in Rats, Anal. Chem. **85** 10949–10955 (2013).
[28] S. Kim, E.Y. Jang, S.-H. Song, J.S. Kim, I.S. Ryu, C.-H. Jeong, S. Lee, Brain Microdialysis Coupled to LC-MS/MS Revealed That CVT-10216, a Selective Inhibitor of Aldehyde Dehydrogenase 2, Alters the Neurochemical and Behavioral Effects of Methamphetamine, ACS Chem. Neurosci. **12** 1552–1562 (2021).
[29] H.A. Saputra, M.M. Karim, Enzymatic and Enzyme-Free Electrochemical Lactate Sensors: A Review of the Recent Developments, Electrochem. Sci. Adv. **5** e202400021 (2025).
[30] M.H. Hassan, C. Vyas, B. Grieve, P. Bartolo, Recent Advances in Enzymatic and Non-Enzymatic Electrochemical Glucose Sensing, Sensors **21** 4672 (2021).
[31] F. Poletti, B. Zanfrognini, L. Favaretto, V. Quintano, J. Sun, E. Treossi, M. Melucci, V. Palermo, C. Zanardi, Continuous capillary-flow sensing of glucose and lactate in sweat with an electrochemical sensor based on functionalized graphene oxide, Sens. Actuators B Chem. **344** 130253 (2021).
[32] S. Fande, D. Sriram, S. Goel, Real-time multiplex electrochemical biosensor for simultaneous quantification of glucose and lactate in cell and bodily fluids, Electrochimica Acta **531** 146421 (2025).
[33] T. Yamazaki, T. Ikeda, B. Lim, K. Okumura, M. Ishida, K. Sawada, Smart Integrated Sensor for Multiple Detections of Glucose and L-Lactate Using On-Chip Electrochemical System, J. Sens. **2011** 190284 (2011).
[34] B. Zhu, X. Li, L. Zhou, B. Su, An Overview of Wearable and Implantable Electrochemical Glucose Sensors, Electroanalysis **34** 237–245 (2022).
[35] E. Demir, K.K. Kırboga, M. Işık, Chapter 8 - An overview of stability and lifetime of electrochemical biosensors, in: J.G. Manjunatha (Ed.), Nov. Nanostructured Mater. Electrochem. Bio-Sens. Appl., Elsevier, 129–158 (2024).
[36] K. Golcuk, G.S. Mandair, A.F. Callender, N. Sahar, D.H. Kohn, M.D. Morris, Is photobleaching necessary for Raman imaging of bone tissue using a green laser, Biochim. Biophys. Acta BBA - Biomembr. **1758** 868–873 (2006).
[37] F. De Ridder, R. Braspenning, J.S. Ordonez, G. Klarenbeek, P. Lauwers, K.J. Ledeganck, D. Delbeke, C. De Block, Early feasibility study with an implantable near-infrared spectroscopy sensor for glucose, ketones, lactate and ethanol, PLOS ONE **19** e0301041(2024).
[38] Z. Li, H. Lv, T. Li, G. Si, Q. Wang, J. Lv, X. Hu, Reagent-free simultaneous determination of glucose and cholesterol in whole blood by FTIR-ATR, Spectrochim. Acta. A. Mol. Biomol. Spectrosc. **178** 192–197 (2017).
[39] T. Koyama, N. Shibata, S. Kino, A. Sugiyama, N. Akikusa, Y. Matsuura, A Compact Mid-Infrared Spectroscopy System for Healthcare Applications Based on a Wavelength-Swept, Pulsed Quantum Cascade Laser, Sensors **20** 3438(2020).
[40] L. Christie, S. Rutherford, D.S. Palmer, M.J. Baker, H.J. Butler, Bioprocess monitoring applications of an innovative ATR-FTIR spectroscopy platform, Front. Bioeng. Biotechnol. **12** 1349473 (2024).
[41] S. Yu, D. Li, H. Chong, C. Sun, H. Yu, K. Xu, In vitro glucose measurement using tunable mid-infrared laser spectroscopy combined with fiber-optic sensor, Biomed. Opt. Express **5** 275–286 (2014).

[42] R. Lu, W.-W. Li, B. Mizaikoff, A. Katzir, Y. Raichlin, G.-P. Sheng, H.-Q. Yu, High-sensitivity infrared attenuated total reflectance sensors for in situ multicomponent detection of volatile organic compounds in water, Nat. Protoc. **11** 377–386 (2016).
[43] H.M. Heise, L. Küpper, L.N. Butvina, Mid-infrared attenuated total reflection spectroscopy of human stratum corneum using a silver halide fiber probe of square cross-section and adhesive tape stripping, J. Mol. Struct. **661** 381–389 (2003).
[44] S. Basov, Y. Dankner, M. Weinstein, A. Katzir, M. Platkov, Technical Note: Noninvasive mid-IR fiber-optic evanescent wave spectroscopy (FEWS) for early detection of skin cancers, Med. Phys. **47** 5523–5530 (2020).
[45] I.L. Jernelv, K. Strøm, D.R. Hjelme, A. Aksnes, Mid-infrared spectroscopy with a fiber-coupled tuneable quantum cascade laser for glucose sensing, in: Opt. Fibers Sens. Med. Diagn. Treat. Appl. XX, SPIE, 105–113 (2020).
[46] T.-A. Lee, Z. Xiao, D.P. Burghoff, T. Hutter, Mid-infrared spectroscopy on a fiber tip for molecular monitoring, Opt. Eng. **64** 076102 (2025).
[47] T.-A. Lee, R. Gonzales, T. Hutter, Parametric study of a microdialysis probe and study of depletion effect using ethanol as a test analyte, Biochem. Biophys. Res. Commun. **637** 136–143 (2022).
[48] J. Ren, Z. Li, F.-S. Wong, A new method for the prediction of pore size distribution and MWCO of ultrafiltration membranes, J. Membr. Sci. **279** 558–569 (2006).
[49] E.K. Plyler, Infrared spectra of methanol, ethanol, and n-propanol, J. Res. Natl. Bur. Stand. **48** 281 (1952).
[50] J.-J. Max, C. Chapados, Glucose and Fructose Hydrates in Aqueous Solution by IR Spectroscopy, J. Phys. Chem.
[51] J.D.S. Goulden, Infra-red spectra of lactates in aqueous solution, Spectrochim. Acta **16** 715–720 (1960).
[52] S. Delbeck, L.K. Iv, S. Delbeck, H.M. Heise, Applications of tapered flat silver halide fiber elements for infrared biospectroscopy with aspects of optical stability and biocompatibility, in: Opt. Fibers Sens. Med. Diagn. Treat. Appl. XVIII, SPIE, 84–96 (2018).
[53] N.H.G. Holford, Clinical Pharmacokinetics of Ethanol, Clin. Pharmacokinet. **13** 273–292 (1987).
[54] J.R.M. Franckson, W. Malaise, Y. Arnould, E. Rasio, H.A. Ooms, E. Balasse, V. Conard, P.A. Bastenie, Glucose kinetics in human obesity, Diabetologia **2** 96–103 (1966).
[55] J.-L. Vincent, A. Quintairos e Silva, L. Couto, F.S. Taccone, The value of blood lactate kinetics in critically ill patients: a systematic review, Crit. Care **20** 257 (2016).
[56] L. Kvitek, A. Panacek, R. Prucek, J. Soukupova, M. Vanickova, M. Kolar, R. Zboril, Antibacterial activity and toxicity of silver – nanosilver versus ionic silver, J. Phys. Conf. Ser. **304** 012029 (2011).
[57] H.A. Olszowy, J. Rossiter, J. Hegarty, P. Geoghegan, Background levels of bromide in human blood, J. Anal. Toxicol. **22** 225–230 (1998).
[58] S.K. Raut, K. Singh, S. Sanghvi, V. Loyo-Celis, L. Varghese, E.R. Singh, S. Gururaja Rao, H. Singh, Chloride ions in health and disease, Biosci. Rep. **44** BSR20240029 (2024).

ACKNOWLEDGEMENTS

Research reported in this publication was supported by the National Institute on Alcohol Abuse and Alcoholism (NIAAA) of the National Institutes of Health (NIH) under Award Number R21AA029770 (T.H.). The content is solely the responsibility of the authors and does not necessarily represent the official views of the National Institutes of Health. T.-A.L. would like to acknowledge the financial support provided by the Fred Murphy Jones and Homer Lindsey Bruce Endowed Fellowship from the Waggoner Center for Alcohol and Addiction Research at The University of Texas at Austin.

AUTHOR CONTRIBUTIONS STATEMENT

T.-A.L: Conceptualization, Data curation, Formal analysis, Investigation, Methodology, Visualization, Writing – original draft; **T.H**: Conceptualization, Funding acquisition, Project administration, Resources, Supervision, Writing – review and editing.

COMPETING INTEREST

The authors declare that Tanya Hutter and Tse-Ang Lee are inventors on a pending and unpublished U.S. provisional patent application (No. 63/749,262) related to the work described in the manuscript, and it is owned by The University of Texas at Austin.

TABLES

Table 1. Physiological levels, clinical relevance, importance of simultaneous monitoring and applications for ethanol, glucose and lactate.

Compound	Typical physiological concentration in tissue	Clinical and physiological significance	Importance of multi-analyte monitoring	Applications
Ethanol	Negligible under normal conditions; can reach 100 mM during intoxication [12].	Relevant in intoxication, addiction, brain injury [13]; influences glucose and lactate metabolism [9]; significant for understanding neural effects and systemic toxicity [14].	Ethanol alters glucose and lactate levels due to hepatic metabolic competition and mitochondrial effects [9,10]; combined monitoring provides insights into metabolic disruption during alcohol exposure or injury.	Addiction treatment, forensic toxicology, ICU monitoring, alcohol-related brain injury research.
Glucose	~3–9 mM in blood and in interstitial fluid [15].	Essential source of energy [16]; critical for brain metabolism [16]; primary target in diabetes management [6]; changes indicate metabolic dysfunction after traumatic brain injury [17].	Glucose metabolism is linked to lactate production via glycolysis [18]; ethanol metabolism competes with glucose utilization and affects blood glucose regulation [10].	Diabetes monitoring, metabolic studies, traumatic brain injury assessment.
Lactate	~0.3–1.3 mM under normal conditions [19]; elevated (>5 mM) in hypoxia, sepsis, trauma [19].	Indicator of anaerobic metabolism [20]; elevated levels signal tissue hypoxia, sepsis, or metabolic stress [21]; serves as a prognostic marker in critical care[22].	Ethanol metabolism alters NAD^+/NADH balance, impacting lactate levels [23]; lactate rises when glucose metabolism is impaired [24].	Sepsis monitoring, trauma evaluation, sports medicine, metabolic research.

Table 2. Prediction of concentration of each compound in the mixture. Values are presented as mean ± relative standard error.

Compound	Mixture 1		Mixture 2		Mixture 3	
	Actual concentration (mM)	Predicted concentration (mM)	Actual concentration (mM)	Predicted concentration (mM)	Actual concentration (mM)	Predicted concentration (mM)

Ethanol	20	22.1 ± 5.8%	10	9.0 ± 6.7%	10	11.2 ± 4.5%
Glucose	10	9.2 ± 3.3%	20	19.3 ± 4.7%	10	9.6 ± 4.2%
Lactate	10	10.4 ± 2.9%	10	10.3 ± 3.9%	20	20.4 ± 3.4%

Table 3. Relative standard error (RSE) of the peak heights used for quantifying ethanol, glucose and lactate. RSE was calculated using peak heights measured as individual components and multi-compound mixtures at 10 and 20 mM concentrations.

	RSE of ethanol peak height		**RSE of glucose peak height**		**RSE of lactate peak height**	
	Individual (%)	In mixture (%)	Individual (%)	In mixture (%)	Individual (%)	In mixture (%)
10 mM	3.4	8.9	3.0	4.0	2.2	3.1
20 mM	2.3	5.9	2.7	4.6	3.4	3.5

FIGURE CAPTIONS

Figure 1. FTIR absorbance spectra of (a) ethanol, (b) glucose and (c) lactate in aCSF at various concentrations between 2.5 and 40 mM measured with a pathlength of 50 μm. (d) Calibration curve showing peak heights versus concentration for each compound. Error bars represent the standard deviation (N=3).

Figure 2. Transflection fiber probe measurements and calibration of ethanol, glucose and lactate. Absorbance of (a) ethanol, (b) glucose, and (c) lactate in aCSF measured using the mid-IR transflection fiber probe with an averaged optical pathlength of 63 μm. (d) Calibration curve showing peak height versus concentration for each compound. Error bars represent the standard deviation (N=3)

Figure 3. Quantification of mixture of ethanol, glucose and lactate using peak deconvolution. (a) Absorbance spectrum of a mixture containing 20 mM ethanol, 20 mM glucose, and 20 mM lactate measured using the fiber probe with an averaged optical pathlength of 63 μm, overlaid with the peak deconvolution fit. (b) Absorbance spectra of three different mixtures with varying concentrations of glucose, lactate and ethanol used to validate the deconvolution method.

Figure 4. Performance comparison with and without a semi-permeable membrane. (a) Calibration curves for glucose in aCSF obtained using the probe with and without the semi-permeable membrane. Time-course infrared peak height at 1036 cm^{-1} of 20 mM glucose measured using the fiber probe (b) without and (c) with a semi-permeable membrane. The shaded region indicates the period when the probe was immersed in the glucose solution. Error bars represent the standard deviation (N=3).

Figure 5. Fiber probe measurements in *ex vivo* skin and comparison with microdialysis. (a) Time-course comparison of ethanol measurements in the skin samples using fiber probe and microdialysis. Ethanol was spiked into the medium at t = 0 min to achieve a final concentration of 20 mM. (b) Simultaneous monitoring of ethanol,

glucose, and lactate in the skin sample, with the medium spiked at 100 mM for each compound. (c) Monitoring of ethanol dynamics in the skin sample following the injection of 50 μL of 200 mM ethanol at t = 0 min. A rapid increase in ethanol concentration was observed, followed by dilution at t = 30 min with the addition of 20 μL of medium.

Figure 6. Silver ion concentration released from the silver halide fiber probe with a semi-permeable membrane immersed in ultrapure water over seven days.

Figure 7. Schematic of the transflection fiber probe and experimental setup. (a) Configuration of the transflection fiber probe. (b) Photograph of the probe. (c) Schematic of the optical setup for the transflection probe measurements. (d) Schematic of the experimental setup using *ex vivo* skin. Both the transflection fiber probe and lab-made microdialysis probe were inserted into the dermis and secured in place, with the setup maintained at 37^{o}C. The photograph on the right shows the fiber probe (left) and microdialysis probe (right) inserted in the human skin sample inside the cell culture insert. (e) Schematic of the injection experiment, where ethanol was injected into the skin near the probe.

Editorial summary:
This study reports a 1.1-mm diameter mid-infrared transflection fiber probe, the smallest reported to date, enabling label-free, simultaneous detection of ethanol, glucose, and lactate, with validation in ex vivo human skin and comparison to microdialysis.

Peer review information: *Nature Communications* thanks Markus W. Sigrist, and the other, anonymous, reviewer(s) for their contribution to the peer review of this work. A peer review file is available.